Competing magnetic phases in mixed-valent manganese oxide perovskites

G.-L. Liu, J.-S. Zhou, and J. B. Goodenough
Texas Materials Institute, ETC 9.102, The University of Texas at Austin, 1 University Station, C2201, Austin, Texas 78712, USA
(Received 28 May 2004; published 16 December 2004)

Measurement of specific heat $C_p(T)$ below 300 K of melt-grown samples of $La_{1-x}Ca_xMnO_3$ ($0 \leqslant x \leqslant 0.3$) and $R_{0.7}A_{0.3}MnO_3$ (R=rare-earth, A=alkaline-earth) with room-temperature tolerance factor $0.950 \leqslant t \leqslant 0.996$ have been supplemented by transport and magnetic measurements. Comparison of the phase diagram of $La_{1-x}Ca_xMnO_3$ with that of $La_{1-x}Sr_xMnO_3$ and the evolution with t of the $R_{0.7}A_{0.3}MnO_3$ family illustrate the sensitivity to t of the crossover from localized to itinerant behavior of the σ-bonding electrons and support the model of two magnetic phases in the crossover compositional range that has been used to account for the colossal magnetoresistance (CMR) phenomenon found in these oxides. A vanishing of the specific-heat anomaly at the Curie temperature T_c and the magnetic data at crossover are typical of a spin glass, and a broad hump in $C_p(T)$ below a $T_h > T_c$, where there is no anomaly at the T_c signal ferromagnetic ordering within isolated pockets of a hole-rich, conductive O* minority phase at T_h. On cooling through T_N of the antiferromagnetic matrix, the spins freeze at a spin-glass temperature T_g in zero magnetic field H if the ferromagnetic phase does not percolate; the ferromagnetic phase grows in an applied H, and a modest H converts the spin glass to a bulk ferromagnet with a Curie temperature $T_c \approx T_g$, where the ferromagnetic phase grows to beyond percolation. As x increases in $La_{1-x}Ca_xMnO_3$, a ferromagnetic-insulator O″ phase having a charge ordering and a different orbital ordering than the parent O′ phase percolates below a $T_g \approx T_c$, and the minority O′ phase remains paramagnetic until it becomes antiferromagnetic below a $T_M < T_c \approx T_g$. In the interval $0.15 < x < 0.25$, an orbitally disordered conductive, ferromagnetic vibronic phase appears in a narrow temperature interval $T_{oo} < T < T_c$, the majority phase transforming to the charge and orbitally ordered O″ phase below a T_{oo}. At $x \geqslant 0.25$, the system transforms from a polaronic paramagnetic to a ferromagnetic metal at T_c.

DOI: 10.1103/PhysRevB.70.224421 PACS number(s): 75.50.Lk, 71.70.Ej, 71.70.Gm, 75.40−s

I. INTRODUCTION

The manganese-oxide perovskites $La_{1-x}A_xMnO_3$ and $R_{0.7}A_{0.3}MnO_3$ (A=alkaline earth and R=rare-earth) have been studied extensively because they exhibit unusual physical properties as a result of a crossover from localized to itinerant electronic behavior of σ-bonding 3d electrons in the presence of localized π-bonding 3d electrons on the manganese ions. The parent compounds $RMnO_3$ contain octahedral-site Mn(III) ions with localized high-spin configurations t^3e^1, but the e-orbital degeneracy is removed by cooperative oxide-ion displacements. These displacements are static and long-range-cooperative giving an O′-orthorhombic axial ratio $c/a < \sqrt{2}$ below an orbital-ordering temperature T_{JT}; they are short-range and fluctuating above T_{JT} where they give an O*-orthorhombic axial ratio $c/a \approx \sqrt{2}$. Regions of short-range fluctuations set in above a $T^* < T_{JT}$ in $LaMnO_3$.[1]

The ideal $RMnO_3$ perovskite structure would consist of a cubic array of corner-shared $MnO_{6/2}$ octahedra with the larger R^{3+} cation at the body center, which has dodecahedral oxygen coordination. Mismatch of the R-O and Mn-O equilibrium bond lengths is given by the deviation from unity of the tolerance factor $t \equiv (R\text{-O})/\sqrt{2}\,(\text{Mn-O})$. The $RMnO_3$ perovskites adjust to a $t < 1$ by cooperative rotations of the $MnO_{6/2}$ octahedra about a cubic [111] or a [110] axis to give, progressively with decreasing t, rhombohedral then orthorhombic symmetry. These rotations bend the Mn-O-Mn bond angle from 180°, and the strength of the σ-bond $(180° - \phi)$ Mn-O-Mn interactions decreases as the bending angle ϕ increases. As the ionic radius of the R^{3+} ion increases to La^{3+}, the transition from localized-e to itinerant-σ^* electrons is approached from the localized-electron side.[2] Oxidation of the MnO_3 array by the introduction of a larger alkaline-earth ion Ca^{2+} or Sr^{2+} increases t and introduces mixed-valent conduction, which induces crossover from localized-e to itinerant-σ^* electrons with increasing Mn(IV) concentration, but the crossover compositional range varies with the tolerance factor. The first-order O′ to O* structural change occurs at a lower temperature and the interval $T^* < T < T_{JT}$ increases as x increases in the $La_{1-x}Ca_xMnO_3$.[3] Moreover, the critical tolerance factor for the transition from polaronic to itinerant behavior above a ferromagnetic Curie temperature T_c is higher than that from vibronic to itinerant behavior below T_c. In this paper, we report specific-heat, transport, and magnetic measurements used to study the crossover in the $La_{1-x}Ca_xMnO_3$ system for comparison with our earlier study on the $La_{1-x}Sr_xMnO_3$ system.[4] We also examined the crossover for a fixed ratio Mn(IV)/Mn=0.3 in compositions $R_{0.7}A_{0.3}MnO_3$ by varying the mean size of the R^{3+} and A^{2+} ions and therefore the tolerance factor t.

II. EXPERIMENTAL PROCEDURES

Melt-grown samples of $La_{1-x}Ca_xMnO_3$ and eight samples of $R_{0.7}A_{0.3}MnO_3$ were grown by the floating-zone method in an IR-radiation image furnace. The polycrystalline feed rods were prepared from a stoichiometric mixture of R_2O_3, Mn_2O_3, and ACO_3 that had been calcined three times at 1050 °C with intermediate grinding. The resulting powder was pressed into a rod and sintered at 1350 °C for 24 h. With $x < 0.25$, the $La_{1-x}Ca_xMnO_3$ rods melted congruently in

TABLE I. Magnetization at 5 K and 50 kOe for $R_{0.7}A_{0.3}MnO_3$.

No.	Composition	M(5 K, 50 kOe) (μ_B/Mn site)	Tolerance factor
1	$La_{0.2}Y_{0.5}Ca_{0.3}MnO_3$	1.8	0.949
2	$Nd_{0.7}Ca_{0.3}MnO_3$	3.7	0.956
3	$Nd_{0.35}Pr_{0.35}Ca_{0.3}MnO_3$	3.6	0.958
4	$Pr_{0.7}Ca_{0.3}MnO_3$	2.9	0.959
5	$La_{0.5}Pr_{0.2}Ca_{0.3}MnO_3$	3.6	0.966
6	$La_{0.6}Pr_{0.1}Ca_{0.3}MnO_3$	3.8	0.967
7	$La_{0.7}Ca_{0.3}MnO_3$	3.7	0.969
8	$La_{0.7}Sr_{0.15}Ca_{0.15}MnO_3$	3.6	0.974
9	$La_{0.7}Sr_{0.3}MnO_3$	3.7	0.979
10	$La_{0.7}Ba_{0.3}MnO_3$	3.6	0.997

a flow of air; with $x>0.25$, they melted congruently in a flow of O_2. Similarly, the $R_{0.7}A_{0.3}MnO_3$ samples could be melted congruently in a flow of air or O_2 depending on composition. This process has been shown to yield stoichiometric samples close to the nominal composition.[1,4,5] The melt-grown samples tend to contain numerous large crystals, but independent measurements on single-crystal specimens showed no difference in the temperature dependence of the resistivity from that reported in the literature,[5] only small difference in the width of the transition at T_c in $La_{0.70}Ca_{0.30}MnO_3$.

Table I lists the compositions of the $R_{0.7}A_{0.3}MnO_3$ family of perovskites; samples No. 1 ($La_{0.2}Y_{0.5}Ca_{0.3}MnO_3$) and No. 10 ($La_{0.7}Ba_{0.3}MnO_3$) were polycrystalline ceramics since the melting zone was found to be unstable for these two compositions. These samples were pressed into rods, sintered, and then cut into several slices with a thickness of $\approx$0.5 mm. For $La_{0.7}Ba_{0.3}MnO_3$, the calcine and sintering temperatures were lowered to 900 °C and 1200 °C, respectively, because of its low melting point.

The temperature dependence of the resistivity $\rho(T)$ was obtained on cooling and warming by four-probe measurements made on bars cut from the melt-grown samples. The critical temperatures were more sharply defined in the melt-grown samples than in the ceramic samples.

The specific heat was measured with the relaxation method.[4,6] The instrument was calibrated by measuring $C_p(T)$ for sapphire and a high-quality single crystal of Fe_3O_4. dc magnetization was obtained with a SQUID (Quantum Design) magnetometer.

III. RESULTS AND DISCUSSION

A. The system $La_{1-x}Ca_xMnO_3$

Figure 1 shows the phase diagram obtained for the system $La_{1-x}Ca_xMnO_3$. The parent compound $LaMnO_3$ is orthorhombic. At room temperature, long-range-cooperative orbital ordering is superimposed on the cooperative octahedral-site rotations about a cubic [110] axis, which lowers the $c/a>\sqrt{2}$ axial ratio in space group *Pbnm* found for

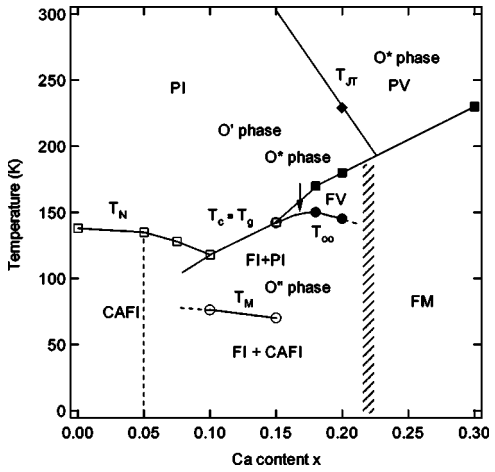

FIG. 1. Phase diagram of the $La_{1-x}Ca_xMnO_3$ system. The open rectangle and circle are from low-field (20 Oe) magnetization; the filled rectangle and circle are from resistivity data; the filled diamond is from a specific-heat measurement. The magnetically ordered two-phase region extends between the two vertical dashed lines.

octahedral-site rotations alone to $c/a<\sqrt{2}$; *a* $c/a>\sqrt{2}$ is designated O-orthorhombic to distinguish it from the O′-orthorhombic $c/a<\sqrt{2}$ phase containing long-range static orbital ordering. At temperatures $T>T_{JT}\approx 750$ K, orbital disorder gives a pseudocubic $c/a\approx\sqrt{2}$, which is designated O*-orthorhombic. A $T^*\approx 600$ K found in $LaMnO_3$ marks the onset of regions of orbital disorder, and c/a increases with T in the range $T^*<T<T_{JT}$.[7] Van Aken *et al.*[3] have reported structural data confirming the two-phase character in this temperature interval. Vibronic superexchange is found in the orbitally disordered phase not only above T_{JT}, as is demonstrated by the $\chi(T)$ data for $LaMnO_3$, but also in the orbitally disordered phase, where phase separation occurs in the interval $T^*<T<T_{JT}$. The transition to the ferromagnetic metallic phase at $x>x_c\approx 0.22$ occurs at the transition from vibronic to itinerant electronic behavior. In the itinerant-electron phase, Jahn-Teller ordering and orbital fluctuations are totally suppressed and de Gennes double exchange is operative. This evolution is consistent with the deduction of Van Aken *et al.*[3] that the transition to the ferromagnetic metallic phase is controlled by the suppression of the Jahn-Teller ordering.

The long-range orbital ordering in $LaMnO_3$ creates long and short Mn-O bond lengths in the (001) planes to give ferromagnetic Mn-O$\cdots$Mn superexchange interactions via the σ-bonding electrons;[8] these ferromagnetic interactions dominate the antiferromagnetic t^3-O-t^3 interactions in these planes and type-A antiferromagnetic order, i.e., ferromagnetic (001) planes coupled antiparallel to one another, is found below a Néel temperature $T_N=145$ K. A Dzialoshinskii antisymmetric superexchange interaction cants the spins below T_N to give a weak ferromagnetic component F_Z; the canted-spin antiferromagnetic insulator (CAFI) is classified as A_yF_z in space group *Pbnm*.[9]

Figure 2 shows the magnetization at 5 K in 50 kOe for $La_{1-x}Ca_xMnO_3$; a smooth transition from the CAFI phase below a T_N to a ferromagnetic phase below a T_c occurs in the

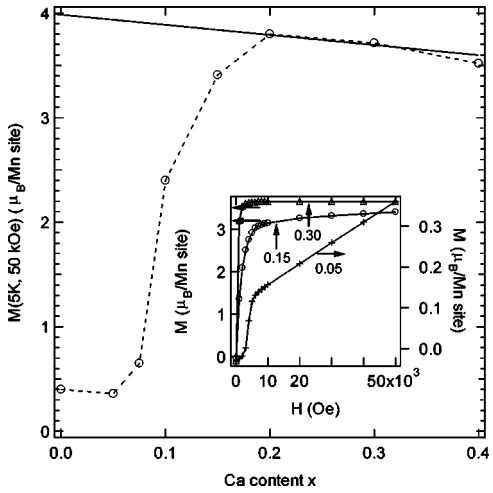

FIG. 2. Magnetization at 5 K in 50 kOe for $La_{1-x}Ca_xMnO_3$, $0 \leqslant x \leqslant 0.4$. Solid line: $(4-x)\ \mu B/Mn$. Inset: $M(5\ K)$ vs applied field. Dashed line is a guide to the eye.

interval $0.08 \leqslant x \leqslant 0.20$. The straight line in Fig. 2 is the theoretical spin-only ferromagnetic magnetization $(4-x)\mu_B/Mn$. The colossal magnetoresistance (CMR) phenomenon is found to reach its maximum above T_c in this same compositional range. There is now extensive evidence[3,10] that an orbitally disordered, conductive O* ferromagnetic phase coexists with the O′ CAFI phase where the CMR phenomenon is found. Above T_c, a minority ferromagnetic phase is embedded in an orbitally ordered paramagnetic insulator (PI) matrix responsible for the O′-orthorhombic structure. The volume fraction of the orbitally disordered ferromagnetic phase grows in an applied magnetic field, and at a sufficiently high field this fraction reaches its percolation threshold to give the CMR phenomenon. We therefore interpret the smooth increase with x in the magnetization at 5 K and in 50 kOe to be due to a smooth increase in the volume fraction of the ferromagnetic phase.

The $\rho(T)$ data of Fig. 3, which are consistent with those in the literature,[11–13] reveal a transition from polaronic to more conductive behavior below T_c as x increases across the interval $0.08 \leqslant x \leqslant 0.20$, but there is a return to semiconductive behavior below a $T_{oo} < T_c$. It has been suggested[3,4] that the upturn in the resistivity signals an alternative orbital and charge ordering that transforms the O* majority ferromagnetic conductive phase into an O″ ferromagnetic insulator (FI) phase. Only in the $x=0.30$ sample did the $\rho(T)$ curve remain metallic to lowest temperatures below T_c. The phase diagram for the $La_{1-x}Sr_xMnO_3$ system[4,14] shows that the transition from the orbital ordering of the PI O′-orthorhombic matrix to that of a low-temperature ferromagnetic insulator (FI) phase passes through a ferromagnetic vibronic (FV) phase in an interval $T_{oo} < T < T_c$, the FV phase appearing in a compositional interval between the CAFI phase and a ferromagnetic metallic (FM) phase. By analogy, we identify the more conductive interval $T_{oo} < T < T_c$ with a percolating FV phase.

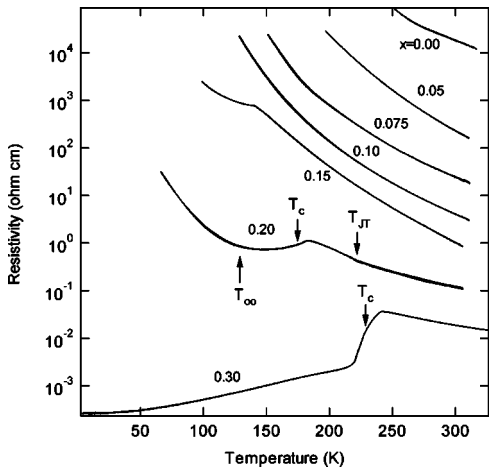

FIG. 3. Resistivity vs temperature for melt-grown samples of the $La_{1-x}Ca_xMnO_3$ system.

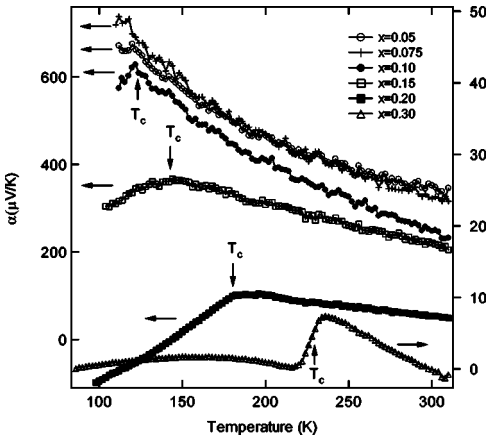

FIG. 4. Thermoelectric power $\alpha(T)$ vs temperature for melt-grown samples of the $La_{1-x}Ca_xMnO_3$ system.

The thermoelectric power $\alpha(T)$ curves of Fig. 4 show that the $x=0.30$ crystal gives a sharp change to metallic behavior below T_c. The resistivity curve for $x=0.30$ of Fig. 3 also shows a sharp change from polaronic to metallic conductivity on cooling through T_c into a ferromagnetic metallic (FM) phase rather than into a FV phase and then into a charge and orbitally ordered FI phase. No attempt was made to obtain data for the compositions in the interval $0.20 < x < 0.30$ where the low-temperature insulator-metal transition occurs. With increasing width of the σ^* band,[15] in the $La_{1-x}Sr_xMnO_3$ system, this transition has been shown to be first-order as is confirmed by the specific-heat data discussed below.

With a two-phase model for the interval $0.05 \leqslant x \leqslant 0.20$, the $\alpha(T)$ curves of Fig. 4 are interpreted to reveal a progressive trapping out with decreasing temperature above T_c of the polaronic charge carriers of the PI matrix by the hole-rich and orbitally disordered ferromagnetic volume fraction. A maximum value of $\alpha(T)$ at T_c in the range $0.10 \leqslant x \leqslant 0.20$ reflects an increase in the concentration of longer-range-mobile charge carriers as the volume fraction of the ferromagnetic phase increases to beyond percolation on cooling through T_c, this volume fraction growing in the internal Weiss molecular field.

Figure 5 compares the specific heat $C_p(T)$ of $La_{1-x}Ca_xMnO_3$ with the magnetizations $M(T)$ obtained in

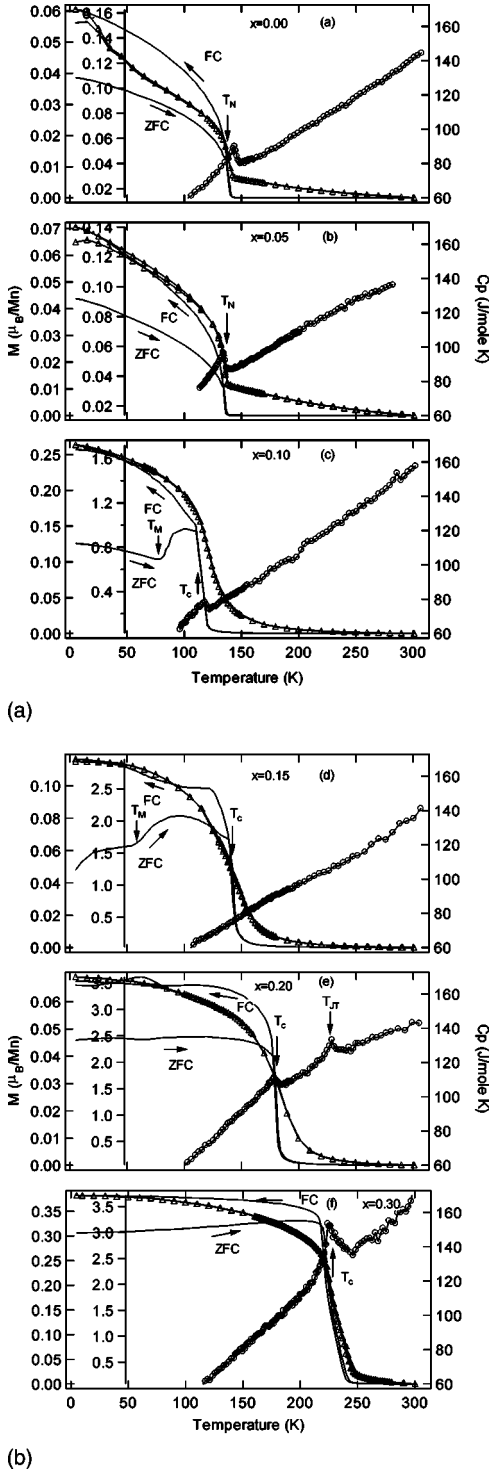

FIG. 5. Magnetization $M(T)$ in $H=20$ Oe and 5 kOe; specific-heat $C_p(T)$ for the $La_{1-x}Ca_xMnO_3$. O=C_p(T), Δ=M(T) in 5 kOe; simple solid line =$M(T)$ in 20 Oe. Arrows indicate warming vs cooling curves.

fields $H=20$ Oe and 5 kOe either on heating after cooling in zero field (ZFC) or on cooling in the measuring field (FC). A correction for the remanent field in the SQUID magnetometer was made to obtain $M(T)$ in a field as low as $H=20$ Oe. The several critical temperatures of Fig. 1 are marked by arrows; they correspond well with transitions found in the $C_p(T)$ and $M(T)$ data.

The $C_p(T)$ data for $x=0.00$ and 0.05 show a typical second-order anomaly at T_N; the weak ferromagnetic moment is due to spin canting. However, $C_p(T)$ for the $x=0.10$ sample has a suppressed entropy change at T_N; considerable short-range magnetic order well above T_N and/or a freezing of the spins at T_N without much change in the long-range order is evident, as can be anticipated where two magnetic phases coexist. We designate T_M in the $x=0.10-0.20$ phases as the temperature where a step increase in $M(T)$ is found on heating the sample in $H=20$ Oe after cooling in zero field. We interpret the transition at T_M to be an antiferromagnetic Néel temperature of a minority O′ phase that is reduced from its value where this phase percolates. Antiferromagnetic order in the minority phase would pin domain walls of the FI majority phase; any pinning by a paramagnetic minority PI phase would be smaller. Papavassiliou *et al.*[16] and Markovich *et al.*[17] have also noted the existence of a magnetic transition in a minority phase at T_M.

The $C_p(T)$ data for $x=0.15$, Fig. 5(d), show a completely suppressed anomaly at T_c, and the $M(T)$ curves in 20 Oe are typical of a spin glass. A step in $M(T)$ at T_M is still visible in the ZFC curve in $H=20$ Oe, but the corresponding FC curve shows an enhancement of $M(T)$ on cooling through T_M; the magnetic order of the spin glass is clearly influenced by even a small applied magnetic field. The existence of a spin-glass phase in this compositional range of the $La_{1-x}Ca_xMnO_3$ system has also been identified by ac susceptibility and a relaxation of the thermo-remanent magnetization.[18] A spin glass is normally found where an antiferromagnetic matrix has its T_N lower than the T_c of an embedded ferromagnetic minority phase below its percolation threshold. In the present case, the ferromagnetic minority phase above T_c appears to grow to its percolation threshold on cooling through T_c so as to shrink the antiferromagnetic majority to below its percolation threshold on cooling through T_c. However, at percolation, some antiferromagnetic regions are stabilized between ferromagnetic clusters to give spin glass behavior in $H=0$.

The $C_p(T)$ anomaly at T_c reappears in the $x=0.20$ and 0.30 samples where the ferromagnetic volume fraction at T_c exceeds a percolation threshold. In the $x=0.20$ sample, a second anomaly in $C_p(T)$ appears at the O′ to O* transition temperature T_{JT}; in the $x=0.30$ samples, the polaronic to itinerant electronic transition on cooling through T_c gives a large entropy change. The temperature T_{JT} decreases from 750 K in $LaMnO_3$ to T_c at $x\approx0.24$ in the $La_{1-x}Ca_xMnO_3$ system; a $T_{JT}=T_c$ is found at $x=0.15$ in the $La_{1-x}Sr_xMnO_3$ system.[4] The shift to a higher value of x in $La_{1-x}Ca_xMnO_3$ is caused by the smaller tolerance factor in the $La_{1-x}Ca_xMnO_3$ system, which narrows the σ^* band.

B. The $R_{0.7}A_{0.3}MnO_3$ family

Figure 6 shows the Curie temperature T_c versus the room-temperature tolerance factor as calculated from ionic radii tabulated by Shannon and Prewitt;[19] the average radius $\langle r_A\rangle$ of the A-site cations, also shown, was calculated for 12-fold oxygen coordination. The Curie temperature was taken as the

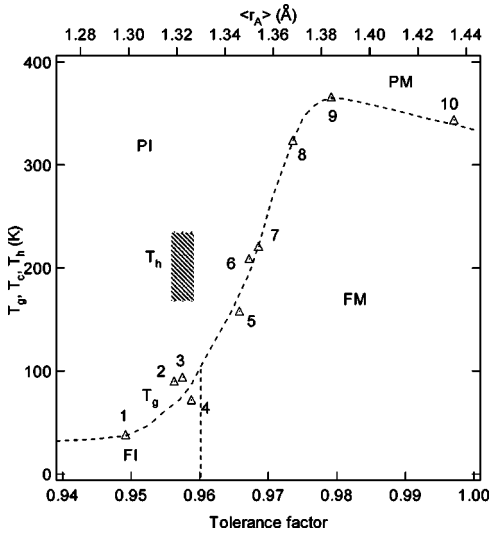

FIG. 6. Phase diagram of the spin freezing temperature T_g and Curie temperature T_c vs tolerance factor for the system $R_{0.7}A_{0.3}MnO_3$; R is one or more trivalent rare earth ions such as La, Y, Nd, or Pr and A is a divalent alkaline earth ion. The T_g, T_c values are from magnetization data. The specific-heat $C_p(T)$ curves of sample No. 2 to No. 4 exhibit a broad hump below a $T_h > T_c$. The vertical line at $t=0.96$ separates the ferromagnetic insulator and metallic (FI and FM) phases as determined by resistivity measurements. Refer to Table I for sample numbers.

point of maximum slope of the $M(T)$ curve obtained on cooling in $H=20$ Oe. From Fig. 7, the vertical dashed line at $t=0.96$ in Fig. 6 separates insulator and metallic domains in the ferromagnetic regions. The width of the σ^* band increases with t, and the crossover compositions from an orbitally ordered insulator phase to an orbitally disordered conductive phase are characterized by the coexistence of the two phases. The vertical dashed line at $t=0.96$ marks where the volume fraction of the conductive phase exceeds its percolation threshold. The volume fraction of the conductive phase is smaller in the paramagnetic region, so crossover is shifted to higher t values above T_c. Since T_c is above 300 K in samples No. 8–No. 10, the $\rho(T)$ data of Fig. 7 do not pinpoint where the paramagnetic phase becomes metallic, but it occurs near $t=0.98$. Compositions No. 9 ($La_{0.7}Sr_{0.3}MnO_3$) and No. 10 ($La_{0.7}Ba_{0.3}MnO_3$) show a metal-metal transition on crossing T_c.[20]

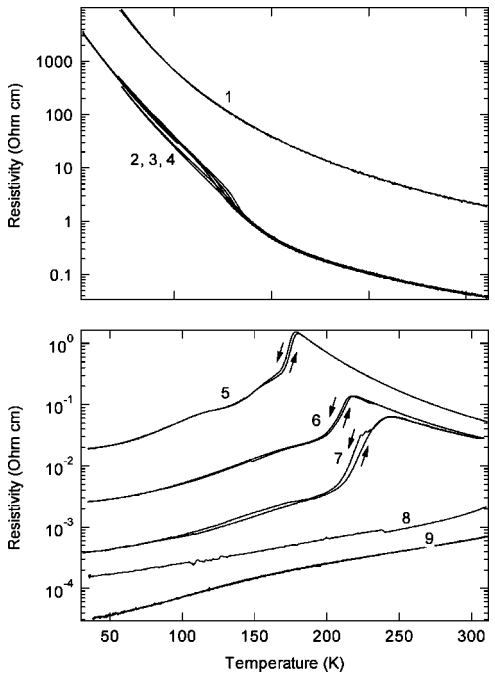

FIG. 7. Resistivity vs temperature for the $R_{0.7}A_{0.3}MnO_3$ system. Arrows refer to heating vs cooling runs. Refer to Table I for sample composition.

The thermal hysteresis of the $\rho(T)$ curves for samples No. 2–No. 7 with tolerance factors $0.955 < t < 0.975$ signals that the magnetic transition at T_c is first-order. It has been argued from the virial theorem[21] that the transition from localized, orbitally ordered electrons to the conductive ferromagnetic phase is first-order; the transition at T_c is first-order where two phases coexist and the volume fraction of one phase increases discontinuously with respect to the other at T_c. In samples No. 5–No. 7, a discontinuous increase in the volume fraction of the FM phase on cooling through T_c causes $\rho(T)$ to drop; the drop in $\rho(T)$ is smooth despite the first-order character of the transition because the volume change causes a crossing of the percolation threshold. In samples No. 2–No. 4, on the other hand, a discontinuous increase in the volume fraction of the FI phase causes $\rho(T)$ to increase. Charge and orbital ordering in the ferromagnetic FI phase appears to occur only below T_c in these samples.

The $\rho(T)$ curves of Fig. 7 and the extraordinary increase in T_c with increasing tolerance factor on traversing the crossover from localized to itinerant σ^* electrons in the MnO_3 array is consistent with data in the literature such as were first reported by Hwang *et al.*[22] In all these samples, the Mn(IV)/Mn ratio is fixed, and the smooth increase in T_c reflects a change in the volume fraction of vibronic superexchange and de Gennes double-exchange interactions; orbital disorder allows 3D ferromagnetic coupling via a vibronic superexchange.[23] Similarly, the smooth decrease in $\rho(T)$ with increasing t reflects an increase in the volume fraction of the more conductive phase as well as a change from small polarons to two-manganese Zener polarons in the paramagnetic matrix as t increases.[10] The sensitivity of $\rho(T)$ to the tolerance factor is reflected in the overlap of the $\rho(T)$ curves for samples No. 2–No. 4, all of which have similar t values. The resistivity of sample No. 1, $La_{0.2}Y_{0.5}Ca_{0.3}MnO_3$, is highest because it is a polycrystalline sample.

Table I lists the magnetizations of the $R_{0.7}A_{0.3}MnO_3$ family at 5 K under a field $H=50$ kOe. The theoretical spin-only value for ferromagnetic saturation is 3.7 μ_B/Mn for a ratio Mn(IV)/Mn=0.3. This value is approached for all samples but No. 1 ($La_{0.2}Y_{0.5}Ca_{0.3}MnO_3$) and No. 4 ($Pr_{0.7}Ca_{0.3}MnO_3$). The 1.8 μ_B/Mn for No. 1 is close to that given by Hwang *et al.*[22] In this sample, the effective ferromagnetic volume fraction remains about 0.5 at 5 K in $H=50$ kOe. Figure 8 shows that $Pr_{0.7}Ca_{0.3}MnO_3$ also retains an effective ferromagnetic volume fraction of only about 0.5 for fields $H \leqslant 35$ kOe, but at $H=40$ kOe the magnetization shows a large step increase, which suggests that some ferromagnetic regions are coupled antiferromagnetically by a retained antiferromagnetic phase;

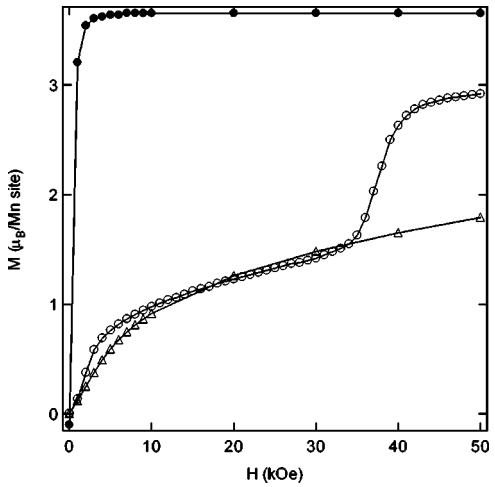

FIG. 8. Magnetization at 5 K vs applied field for melt-grown samples of the $La_{0.7}Ca_{0.3}MnO_3$ (solid circle), $Pr_{0.7}Ca_{0.3}MnO_3$ (open circle), and $La0.2Y_{0.5}Ca_{0.3}MnO_3$ (open triangle).

these regions are rotated in a strong magnetic field against the exchange fields at the two-phase interface to give a metamagnetic component. A similar phenomenon has been observed in $La_{5/8-y}Pr_yCa_{3/8}MnO_3$ with $y=0.35$;[24] it is characteristic of a spin glass.

Figure 9 compares the ZFC and FC $M(T)$ curves in $H=20$ Oe and 50 kOe with the specific heat $C_p(T)$. The specific heat was not measured for sample No. 1 because polycrystalline samples are poor thermal conductors. The low value of $M(20\ \text{Oe})$ for this sample is typical for a CAFI matrix; but the appearance of a significant $M(5\ \text{K})$ in 5 kOe signals the presence of a ferromagnetic minority phase having a volume fraction that increases with the strength of an applied magnetic field. Stabilization by an H field of an orbitally disordered ferromagnetic phase relative to an orbitally ordered CAFI phase has been demonstrated in the system $LaMn_{1-x}Ga_xO_3$.[23]

The $C_p(T)$ curves of samples No. 2–No. 4 exhibit a broad hump below a $T_h > T_c$ and no anomaly at T_c. Magnetic ordering within isolated pockets of a ferromagnetic minority phase would give a broad hump in the $C_p(T)$ curve; and the absence of an anomaly at T_c signals that, in the absence of an applied magnetic field, $T_c \approx T_g$ is a spin-glass freezing temperature. The ZFC $M(T)$ curves are typical of a spin glass, and the compositions all exhibit the CMR phenomenon in the interval $T_c < T < T_h$. The data support the two-phase model for the CMR phenomenon and imply that the CMR phenomenon should begin to be manifest below T_h.

Samples No. 5 and No. 6 exhibit a T_c that approaches T_h as t increases, and a broad $C_p(T)$ anomaly in the range $T_c < T < T_h$ does not reflect the first-order character of the transition at T_c that is signaled by the thermal hysteresis of $\rho(T)$. A discontinuous change in the volume fraction of the orbitally ordered and disordered phases at T_c is not reflected in either $C_p(T)$ or $\rho(T)$ in a heating or a cooling run. As the interval $T_c < T < T_h$ decreases with increasing t, the magnitude of the CMR phenomenon is progressively suppressed.[22] In sample No. 7, $La_{0.7}Ca_{0.3}MnO_3$, long-range magnetic order in a percolating ferromagnetic phase occurs at T_c, so there is no $T_h > T_c$.

Our $C_p(T)$ measurements were confined to below room temperature, so we could not demonstrate whether the magnetic ordering in samples No. 8 and No. 9 gives a conventional lambda anomaly in $C_p(T)$. However, superposition of the FC and ZFC curves in $H=20$ Oe shows there is no evidence of spin-glass behavior in these samples. An O*-R transition at $T_{OR} < T_c$ in sample No. 8 is barely visible in the $C_p(T)$ curve; it is more clearly marked by a step in $M(T)$ taken with $H=20$ Oe and in the resistivity curve of Fig. 7. A thermal hysteresis of the $M(T)$ curves in $H=20$ Oe for FC vs ZFC signals that the O*-R transition is weakly first-order. A similar transition was found in the $La_{1-x}Sr_xMnO_3$ system.[4]

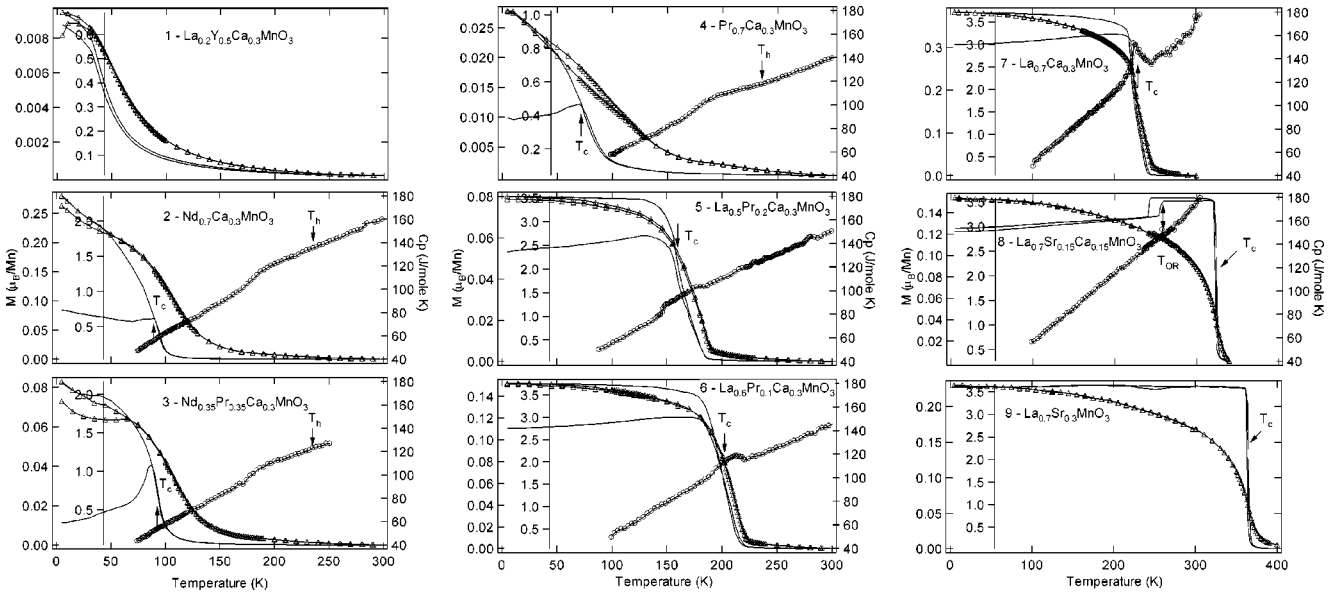

FIG. 9. Magnetization $M(T)$ in $H=20$ Oe and 5 kOe; specific heat $C_p(T)$: O=C_p, Δ=$M(T)$ in 5 kOe; simple solid line =$M(T)$ in 20 Oe. Arrows indicate warming vs cooling curves.

IV. CONCLUSIONS

Measurements below 300 K of the specific heat $C_p(T)$ together with transport and magnetic measurements on the system $La_{1-x}Ca_xMnO_3$ and 10 members of the $R_{0.7}A_{0.3}MnO_3$ family with tolerance factor $0.950 \leqslant t \leqslant 0.996$ have confirmed the coexistence of two magnetic phases where there is a crossover from localized to itinerant character of the σ-bonding $3d$ electrons on the MnO_3 array. Moreover, the range of Mn(IV)/Mn ratios over which two magnetic phases coexist is shown to be more sensitive to the tolerance factor than a tight-binding bandwidth $W \sim \cos\phi$ would predict, as is also made evident by comparison of the $La_{1-x}Ca_xMnO_3$ and $La_{1-x}Sr_xMnO_3$ systems. This sensitivity has been attributed to the vibronic character of the electrons where bond-length fluctuations are present.[25]

The data for the $La_{1-x}Ca_xMnO_3$ system support the following model for the evolution of physical properties below room temperature: $LaMnO_3$ contains localized, high-spin Mn(III): t^3e^1 $3d$-electron configurations, and ordering of the e orbitals by a cooperative Jahn-Teller distortion gives an A_yF_z canted-spin antiferromagnetic-insulator (CAFI) phase. With $x=0.05$ Ca substituted for La, mobile holes are progressively trapped out on lowering the temperature; the traps are presumably a hole-rich and orbitally disordered phase that is identified as the trap site at higher values of x. In the range $0.08 \leqslant x \leqslant 0.20$, the volume fraction of the hole-rich, orbitally disordered phase increases with x, and ferromagnetic ordering within this phase introduces spin-glass behavior where the ferromagnetic phase does not percolate in zero magnetic field ($H=0$); but growth of the ferromagnetic phase to beyond percolation in a modest H field converts the spin glass to a bulk ferromagnetic insulator having a $T_c \approx T_g$ with a magnetization that increases with the volume fraction of the ferromagnetic phase. Growth of the volume fraction of the conductive ferromagnetic phase above T_c dilutes the hole concentration in the phase in $La_{1-x}Ca_xMnO_3$, which would reduce the de Gennes double-exchange coupling, but orbital disorder introduces a 3D vibronic superexchange as in $LaMn_{1-x}Ga_xO_3$. Where the ferromagnetic phase just percolates at T_c, the ferromagnetic conductive vibronic (FV) minority phase above T_c is retained to a charge and orbital ordering temperature $T_{oo} < T_c$ where the FV phase converts to the FI phase. However, the insulator phase is the minority phase below T_c in the range $0.10 \leqslant x \leqslant 0.20$, and antiferromagnetic order in this phase below a $T_M < T_c$ has a weak ferromagnetic component.

Experiments on the $R_{0.7}A_{0.3}MnO_3$ family revealed that as T_g increases with the tolerance factor t to the temperature T_h of the onset of magnetic order within ferromagnetic clusters, the spin glass in $H=0$ converts to a bulk ferromagnetic metal. The CMR phenomenon occurs in the range $T_g < T < T_h$.

ACKNOWLEDGMENTS

We thank the NSF and both the TCSUH and the Robert A. Welch Foundation of Houston, TX for financial support.

[1] J.-S. Zhou and J. B. Goodenough, Phys. Rev. B **60**, R15002 (1999).
[2] J.-S. Zhou and J. B. Goodenough, Phys. Rev. Lett. **89**, 087201 (2002); J.-S. Zhou and J. B. Goodenough, Phys. Rev. B **68**, 054403 (2003).
[3] Bas B. Van Aken, Oana D. Jurchescu, Auke Meetsma, Y. Tomioka, Y. Tokura, and Thomas T. M. Palstra, Phys. Rev. Lett. **90**, 066403 (2003).
[4] G.-L. Liu, J.-S. Zhou, and J. B. Goodenough, Phys. Rev. B **64**, 144414 (2001).
[5] T. Okuda, Y. Tomioka, A. Asamitsu, and Y. Tokura, Phys. Rev. B **61**, 8009 (2000).
[6] G. R. Stewart, Rev. Sci. Instrum. **54**, 1 (1983).
[7] J. Rodriguez-Carvajal, M. Hennion, F. Moussa, A. H. Moudden, L. Pinsard, and A. Revcolevschi, Phys. Rev. B **57**, R3189 (1998).
[8] J. B. Goodenough, Phys. Rev. **100**, 564 (1955).
[9] E. F. Bertaut, in *Magnetism: A Treatise on Modern Theory and Materials*, edited by G. T. Rado and H. Suhl (Academic, New York, 1963), Chap. 4.
[10] J.-S. Zhou and J. B. Goodenough, Phys. Rev. B **62**, 3834 (2000); J. B. Goodenough and J.-S. Zhou Struct. Bonding (Berlin) **98**, 17 (2001), and references therein.
[11] Chang Seop Hong, Wan Seop Kim, and Nam Hwi Hur, Phys. Rev. B **63**, 092504 (2001).
[12] V. Markovich, E. Rozenberg, A. I. Shames, G. Gorodetsky, I. Fita, K. Suzuki, R. Puzniak, D. A. Shulyatev, and Ya. M. Mukovskii, Phys. Rev. B **65**, 144402 (2002).
[13] Guo-meng Zhao, H. Keller, W. Prellier, and D. J. Kang, Phys. Rev. B **63**, 172411 (2001).
[14] J.-S. Zhou, J. B. Goodenough, A. Asamitsu, and Y. Tokura, Phys. Rev. Lett. **79**, 3234 (1997).
[15] J.-S. Zhou, G.-L. Liu, and J. B. Goodenough, Phys. Rev. B **63**, 172416 (2001).
[16] G. Papavassiliou, M. Pissas, M. Belesi, M. Fardis, J. Dolinsek, C. Dimitropoulos, and J. P. Ansermet, Phys. Rev. Lett. **91**, 147205 (2003).
[17] V. Markovich, I. Fita, R. Puzniak, M. I. Tsindlekht, A. Wisniewski, and G. Gorodetsky, Phys. Rev. B **66**, 094409 (2002).
[18] R. Laiho, E. Lahderanta, J. Salminen, K. G. Lisunov, and V. S. Zakhvalinskii, Phys. Rev. B **63**, 094405 (2001).
[19] R. D. Shannon and C. T. Prewitt, Acta Crystallogr., Sect. B: Struct. Crystallogr. Cryst. Chem. **25**, 725 (1969); R. D. Shannon and C. T. Prewitt, *ibid.* **26**, 1046 (1970).
[20] A. Urushibara, Y. Moritomo, T. Arima, A. Asamitsu, G. Kido, and Y. Tokura, Phys. Rev. B **51**, 14103 (1995).
[21] J. B. Goodenough, Aust. J. Phys. **52**, 155 (1999).
[22] H. Y. Hwang, S-W. Cheong, P. G. Radaelli, M. Marezio, and B. Batlogg, Phys. Rev. Lett. **75**, 914 (1995).
[23] J.-S. Zhou, H. Q. Yin, and J. B. Goodenough, Phys. Rev. B **63**, 184423 (2001).
[24] V. Kiryukhin, B. G. Kim, V. Podzorov, S.-W. Cheong, T. Y. Koo, J. P. Hill, I. Moon, and Y. H. Jeong, Phys. Rev. B **63**, 024420 (2000).
[25] J. B. Goodenough and J.-S. Zhou, Mater. Res. Soc. Symp. Proc. **494**, 335 (1998).